Role of Tyrosine-34 in the Anion Binding Equilibria in Manganese(II) Superoxide Dismutases†

Leandro C. Tabares,‡,§ Néstor Cortez,§ and Sun Un*,‡

Service de Bioénergétique, Biologie Structurale et Mécanismes, Institut de Biologie et Technologies de Saclay, CNRS URA 2096, CEA Saclay, 91191 Gif-sur-Yvette, France, and Instituto de Biología Molecular y Celular de Rosario (IBR), Universidad Nacional de Rosario and CONICET, Suipacha 531, S2002LRK Rosario, Argentina

Received March 5, 2007; Revised Manuscript Received May 18, 2007

ABSTRACT: Superoxide dismutases (SODs) are proteins specialized in the depletion of superoxide from the cell through disproportionation of this anion into oxygen and hydrogen peroxide. We have used high-field electron paramagnetic resonance (HFEPR) to test a two-site binding model for the interaction of manganese-SODs with small anions. Because tyrosine-34 was thought to act as a gate between these two sites in this model, a tyrosine to phenylalanine mutant of the superoxide dismutase from *R. capsulatus* was constructed. Although the replacement slightly reduced activity, HFEPR measurements demonstrated that the electronic structure of the Mn(II) center was unaffected by the mutation. In contrast, the mutation had a profound effect on the interactions of fluoride and azide with the Mn(II) center. It was concluded that the absence of tyrosine-34 prevented the close approach of these anions to the metal ion. This mutation also enhanced the formation of a hexacoordinated water−Mn(II)SOD complex at low temperatures. Together, these results showed that the role of Y34 is unlikely to involve redox tuning but rather is important in regulating the equilibria between the anionic substrate in solution and the two binding sites near the metal. These observations further supported the originally proposed mutually exclusive two-binding-site model.

Superoxide dismutases (SODs[1]) play a key role in cellular protection against oxidative damage by catalyzing the disproportionation of superoxide to oxygen and hydrogen peroxide (*1*, *2*). Their cyclic oxidation−reduction mechanism involves a metal cofactor (*3*−*5*). There are four distinct families of SODs distinguishable by the metal cofactor that they use: manganese, iron, copper-zinc (*1*), and nickel (*6*, *7*). In the case of iron, manganese, and nickel SODs, the metal cofactor cycles between its divalent and trivalent oxidation states, whereas in the copper-zinc enzymes, the copper ion cycles between the Cu(I) and Cu(II) oxidation states. Although iron and manganese SODs (FeSODs and MnSODs) exhibit high structural homology (*8*−*11*), their activities are highly metal-specific (*12*, *13*), and only a small subgroup of so-called cambialistic-SODs are active with either metal ion (*14*−*18*). The metal ion in the Fe and MnSODs are coordinated by two histidines and an aspartic acid in the equatorial plane and a histidine and solvent molecule in the axial positions forming a trigonal bipyramidal geometry. The solvent molecule hydrogen bonds both the equatorial aspartate ligand and the amide side chain of a nearby glutamine (Q146 in the MnSOD or Q69 in the FeSOD from *E. coli*), which is also hydrogen bonded to a tyrosine (Y34) residue. This tyrosine is highly conserved in iron and manganese SODs. Studies on the interaction of SODs with small anionic analogues of superoxide suggest that Y34 plays a central role in substrate binding and positioning (*19*−*21*). It has been shown that azide and fluoride bind close but not directly to the Fe(II) centers in reduced FeSODs, forming outer metal sphere complexes, whereas in the oxidized FeSODs, they bond directly to the metal ion, yielding inner sphere complexes (*9*, *19*, *22*−*24*). In contrast, in MnSODs both inner and outer sphere complexes have been observed for both the oxidized and the reduced forms (*21*, *25*, *26*).

Although the replacement of Y34 by phenylalanine has been demonstrated to cause no significant structural changes compared to the wild-type protein (*27*, *28*), this mutation does reduce enzymatic activity (*20*, *29*) and modifies the interactions with azide and fluoride (*19*, *20*), indicating an important role of the phenol group. In particular, it has been shown that in both Fe(III)SOD and Mn(III)SOD Y34F mutants the formation of the inner sphere complexes is favored (*19*, *20*). The same mutation in Fe(II)SODs slightly increased the affinity for azide, but the affinity for fluoride did not appear to be affected (*19*).

Whittaker and Whittaker have studied how replacing Y34 with a phenylalanine affects the interaction of azide, fluoride,

† This work was supported by CEA, CONICET, SeTCIP, ANPCyT, and ECOS Sud/SeCyT Program. L.C.T. and N.C. acknowledge the support of CONICET, SeTCIP and ANPCyT (Argentina); L.C.T, N.C. and S.U. the support from the ECOS Sud/SeCyT collaboration program (Project A02B01); and L.C.T. a postdoctoral position from the CEA.

* To whom correspondence should be addressed. Tel: (33)-169082842. Fax: (33)169088717. E-mail: sun@herode.saclay.cea.fr.

‡ CEA Saclay.

§ Universidad Nacional de Rosario and CONICET.

[1] Abbreviations: SOD, superoxide dismutase; MnSOD, manganese superoxide dismutase; FeSOD, iron superoxide dismutase; RcMnSOD, *Rhodobacter capsulatus* manganese superoxide dismutase; RcMnSOD-WT, RcMnSOD wild type; RcMnSOD-Y34F, RcMnSOD in which Y34 has been replaced by phenylalanine; EPR, electron paramagnetic resonance; HFEPR, High-Field EPR.

10.1021/bi700438j CCC: $37.00
Published on Web 07/18/2007

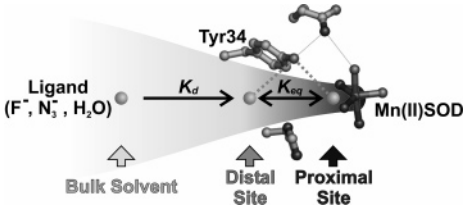

FIGURE 1: Proposed two mutually exclusive binding sites model for anions and water interaction with Mn(II)SODs. The Mn(II) metal-binding site of SODs is shown in conjunction with relevant second sphere amino acids; the residues in the coordination sphere were excluded for clarification. The exogenous ligand present in the bulk solvent (light gray region) interacts with the protein with a given binding constant (K_d). Upon binding, the ligand equilibrates between the distal (gray region) and proximal (dark gray region) sites with an equilibrium constant (K_{eq}).

and cyanide with the reduced MnSOD from *E. coli* (*20*). On the basis of conventional 9 GHz electron paramagnetic resonance (EPR) spectroscopy, they suggested that these anions interact with the reduced protein even after the replacement of Y34 by phenylalanine, but the exact nature of the anion−metal interactions was not clear because of the limited resolution of the conventional 9 GHz EPR measurements (*20*). In contrast, we have shown that by using high-field EPR (HFEPR) it is possible to detect such anion−Mn(II)SOD interactions (*21*, *30*). HFEPR can in a straightforward manner distinguish pentacoordinated Mn(II)SOD, hexacoordinated Mn(II)SOD, and non-protein-bonded Mn(II) ions (*21*). The fundamental difference between the 9 and the 285 GHz EPR is related to the relative magnitudes of observation frequencies and the Mn(II) zero-field interaction of Mn(II)SODs. The Mn(II) zero-field interaction dominates the EPR spectra of Mn(II)SODs and is a consequence of the spin−orbit coupling of the five unpaired electrons and the spin−spin interactions they experience. It is characterized by two parameters D and E, where the former is a measure of the size of the zero-field interaction and the latter, the departure of the interaction from axial symmetry (*21*, *30*, *31*). For MnSODs $|D|$ is about 10 GHz (*30*−*32*). This means that for conventional 9 GHz EPR measurements, the microwave observation frequency and the Mn(II) zero-field interaction are of comparable energy. Under this condition, the spectra are very complex, and it is difficult to extract accurate $|D|$ and E values (*30*, *31*). In contrast, HFEPR uses frequencies that are as much as 30 times larger. The HFEPR spectra are much simpler and more highly resolved and can be used to determine the zero-field interaction with high precision (*30*, *31*).

Using HFEPR spectroscopy, we previously observed two states for azide or fluoride binding to the reduced *E. coli* Mn-type and *R. capsulatus* cambialistic-type SODs (*21*). In both binding-states, these two anions were proposed to interact with Y34. In one case the anion is positioned away from the metal ion (distal, Figure 1), and in the other, it is positioned toward it (proximal, Figure 1). In the latter case, the azide would be positioned sufficiently close so that it could ligate the Mn ion. If this two-state model were correct, then the replacement of Y34 should have a significant effect on anion binding to the reduced MnSOD. To test this model, the Y34F[2] mutant of the *Rhodobacter capsulatus* cambialistic superoxide dismutase was constructed, and the electronic structure of the reduced Mn(II) ion was explored using 285 GHz HFEPR. To the best of our knowledge, this is the first detailed study of the Y34F mutant in Mn(II)SODs, and it reveals an essential role of Y34 in small anion binding.

EXPERIMENTAL PROCEDURES

Protein Samples. Wild-type MnSOD from *R. capsulatus* was prepared as previously described (*18*). Site-directed mutagenesis was performed with QuikChange Site directed Mutagenesis Kit (Stratagene) according to the supplier's protocols using the previously described pESOD3228 plasmid as the template (*18*) and the double stranded 5′-cctgcaccacaaggcgtttgtcgacaacggc-3′ oligonucleotide as the primer. The modified plasmid was sequenced to confirm that the only changes were the desired ones. The Y34F mutant protein was prepared as described for the wild type (*18*).

Protein concentration was estimated using the theoretical extinction coefficients of 48930 $M^{-1}\cdot cm^{-1}$ and 47440 $M^{-1}\cdot cm^{-1}$ at 280 nm per monomer for the wild-type and mutant proteins, respectively, calculated using the ProtParam program (espasy.org/tools.protparam.html (*33*)) and by the colorimetric Amido Black (*34*) and Bradford (*35*) assays. The colorimetric assays were calibrated using 0−10 μg of bovine serum albumin (Sigma).

Manganese and iron contents were determined by atomic absorption spectrometry on a Perkin-Elmer model 3110 spectrometer. The spectrometer was calibrated using a series of solutions of known metal content obtained by diluting a standard 1020 mg/L manganese (Aldrich) or iron (Sigma) solution from 0 to 100 μg/L of metal in 0.2 M nitric acid. Protein samples (~20 μM) were washed several times by ultrafiltration with 10 mM Tris-HCl buffer previously treated with Chelex 100 to remove metal ion traces (Bio-Rad). In the last washing step, the filtrate was collected in a fresh tube and saved to determine the presence of free metal ions. The samples and filtrates were diluted between 10- and 100-fold in 0.2 M nitric acid before manganese and iron determinations.

Activity Measurements. Activity measurements were carried out using the standard assay of McCord and Fridovich (*36*) in 50 mM phosphate buffer at pH 7.8 at 25 °C. The inhibition of activity by the substrate analogues was measured by the addition of 10 mM azide or fluoride to a protein sample containing all of the required components except for the xanthine oxidase, which was added to start the reaction after 10 min of protein−analogue incubation. The reported activities were based on protein concentration as determined using the Bradford assay. For nondenaturing PAGE, the samples were fully reduced with 10 mM dithiotreitol and 2 mM sodium dithionate before running the gel. Superoxide dismutase activity *in situ* was determined using the NBT/riboflavin assay at pH 7.8 (*37*).

Absorption and High-Field EPR Spectra. Absorption and HFEPR spectra were obtained from protein samples in 10 mM Tris-HCl at pH 7.8 and 0.1 mM EDTA. For analogue binding studies, EDTA was omitted, and 100 mM fluoride

[2] For ease of comparison, the amino acid numbering used throughout this work is that of the *E. coli* SOD that is widely used in the literature. In *R. capsulatus*, the tyrosine that was mutated was in fact Y36.

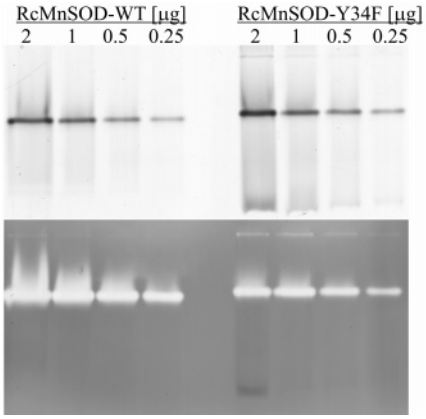

FIGURE 2: Nondenaturing PAGE of RcMnSOD-WT and RcMnSOD-Y34F. Different amounts of purified wild-type and mutant proteins (see details on the figure) were loaded and run in two equivalent PAGE runs under nondenaturing conditions and stained with Coomassie brillant blue for total protein (upper) or with NBT/riboflavin for superoxide dismutase activity (bottom, white spots in the gray background).

or azide was used. Absorption spectra were taken in an Uvikon 992 (Kontron Instruments) spectrophotometer at 298 K. HFEPR samples were flash-frozen in liquid nitrogen from room temperature before spectra were taken. Studies on the temperature dependence of the equilibrium between the penta and hexacoordinated centers (see below) were carried out by incubating samples between 298 and 241 K for 72 h, followed by flash-freezing in liquid nitrogen and acquiring HFEPR spectra. It was determined that after 72 h, the samples were well equilibrated and that at liquid nitrogen temperatures no changes in the relative amounts of the two forms occurred. Adventitious Mn(II) ions and exogenous ligands were removed from the samples using a 5 mL desalting column (Hi-Trap, Amersham Biosciences). Ultrafiltrations were carried out using 30 KDa cutoff membrane filters (Centricon YM-30, Millipore Corporation).

The HFEPR spectrometer has been described in detail elsewhere (*38*). Field calibration was based on a Mn(II)-doped MgO standard sample ($g = 2.000101$ (*39*)), and the absolute error in field measurements was 1 G (0.1 mT) or 0.0001 in g. All spectra were obtained with 10 G modulation under non-saturating conditions at 285 GHz with 5 G resolution at 25 K. The quality of spectra was such that they could be reliably reproduced and singly and doubly integrated.

Simulations of the spectra were carried out as described previously (*31*, *40*). The estimated error limits of the fitting procedure were ± 0.06 GHz for the two zero-field parameters.

Molecular structures were generated using the program PyMOL (Delano Scientific LLC, www.pymol.org).

RESULTS

Expression and Activity of RcMnSOD-Y34F. As with the wild-type *Rhodobacter capsulatus* superoxide dismutase (RcSOD-WT) (*18*), overexpression of the Y34F mutant (RcSOD-Y34F) enzyme in *E. coli* resulted mostly in inclusion body aggregates. These inclusion bodies were purified and dissolved in urea. The resulting denatured apoprotein was refolded in the presence of Mn(II) with similar yield to that of the wild type (*18*). The fully reduced refolded mutant and wild-type proteins showed similar electrophoretic mobilities in nondenaturing gels. The NBT-riboflavin assay for superoxide dismutase activity (*37*, *41*) was carried out at pH 7.8 directly on the gels and showed that the Y34F protein was slightly less active than the wild type (Figure 2). The comparison of the Coomassie-stained and activity-assayed gels suggested that no detectable amounts of apoprotein were present. The apoprotein is intrinsically more negatively charged and should have produced an inactive protein band with a slightly faster electrophoretic mobility than the Mn(II)-containing protein.

Using atomic absorption spectroscopy, it was determined that the extent of manganese incorporation by the RcSOD-WT and RcSOD-Y34F apoproteins refolded in the presence of manganese was essentially complete and that there were no detectable amounts of contaminating iron in either case (less than 1% that of manganese). Moreover, ultrafiltration experiments showed that the protein solutions were free of nonbound manganese ions. Protein concentrations were determined using three different techniques: theoretical extinctions at 280 nm (*33*), the Amido Black assay (*34*), and the Bradford assay (*35*). The manganese contents of the RcSOD-WT and RcSOD-Y34F were determined to be 1.6 ± 0.1 and 1.7 ± 0.1 g-atom of Mn/mol of monomer, respectively, using the theoretical extinction coefficient method; 1.4 ± 0.2 and 1.3 ± 0.1 g-atom of Mn/mol of monomer, respectively, using the Amido Black assay; and 0.9 ± 0.1 and 0.9 ± 0.1 g atom of Mn/mol of monomer, respectively, using the Bradford assay. These measurements indicated that there might have been an excess of manganese. However, the amount of non-active site Mn(II) was low, less than 2% as determined by HFEPR (see below), and any large contributions from non-active site Mn(III) ions seemed unlikely because the HFEPR spectra of samples treated with 2 mM sodium dithionite to reduce Mn(III) to Mn(II) showed only increases in the active-site manganese resonance and no evidence of nonspecifically bound manganese. These spectroscopic data suggest that these methods for determining protein concentration are not without problems and should be used with caution. It is important to note that all three methods showed that the manganese content was the same in wild-type and Y34F samples. Hence, the atomic absorption measurements showed that the differences in activity between the wild type and mutant were unlikely due to the extent of manganese incorporation or the presence of iron. For ease of comparison with our previous work, we have somewhat arbitrarily chosen to report the specific activities based on the Bradford assay.

The specific enzymatic activity of the purified protein was measured by the standard xanthine oxidase/cytochrome *c* assay at pH 7.8 (*36*). The manganese reconstituted mutant protein had an activity of 1321 U/mg or about 27% of the wild-type activity (4883 U/mg). In the presence of 10 mM fluoride, the activity of this mutant was 20% lower, comparable to the 25% reduction observed for the wild-type (RcMnSOD-WT, 3906 U/mg; RcMnSOD-Y34F, 1056 U/mg). In contrast, 10 mM azide appeared to have a bigger inhibitory effect on the mutant with a decrease of 70% in activity compared to 40% for the wild type (RcMnSOD-WT, 2963 U/mg; RcMnSOD-Y34F, 528 U/mg).

Electronic Structure of the Mn(II) Site in the Mutant Protein. The Mn(II) 285 GHz HFEPR spectrum of the Mn-

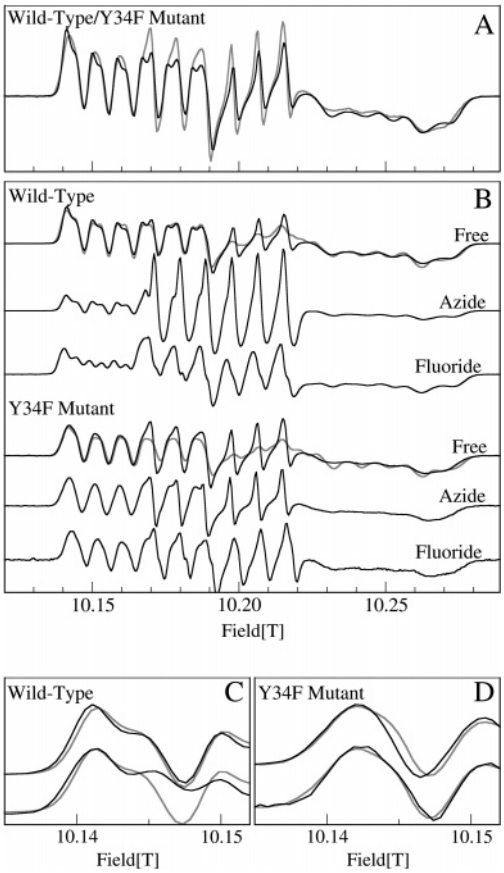

FIGURE 3: HFEPR spectra (285 GHz) of the RcMn(II)SOD-WT and RcMn(II)SOD-Y34F. (A) Comparison between the spectra of the wild-type (black trace) and mutant (gray trace) proteins in normal conditions. (B) Spectra of RcMn(II)SOD-WT (top) and RcMn(II)SOD-Y34F (bottom) were taken in the absence (Free, black trace) or presence of 100 mM sodium azide (Azide) or 100 mM sodium fluoride (Fluoride). The simulation of the spectra in the absence of exogenous ligand for each protein is shown as gray trace. The details of the first resonance for the wild-type (panel C) and mutant (panel D) proteins in the presence of azide (top, black trace) and fluoride (bottom, black trace) are shown superimposed to the spectra of the native proteins (gray trace).

(II)RcSOD-Y34F closely resembled that of the wild-type enzyme, although some differences were detected (Figure 3A). In the low-field region between 10.14 and 10.19 T, each of the resonance lines of the RcMn(II)SOD-WT spectrum presented a shoulder that was not evidenced for RcMn(II)-SOD-Y34F. Above 10.22 T, the spectrum of the mutant protein appeared to be slightly less resolved. Despite these slight differences in line shape, the overall spectral widths were nearly the same for both proteins, indicating that zero-field splitting for the two Mn(II) sites was essentially the same. A simulation of the spectra showed that the $|D|$ and E zero-field parameters were 10.775 and 0.508 GHz, respectively, in RcMn(II)SOD-WT and 10.777 and 0.460 GHz, respectively, for the Y34F mutant (Figure 3B). In both cases, as before with other Mn(II)SODs (*21*, *40*), distributions of 0.100−0.140 GHz in the $|D|$ and E parameters, respectively, were required to obtain good fits. Although the differences between the wild-type and mutant zero-field parameters were within the estimated error of ±0.06 GHz of the fitting procedure, the shift of 0.048 GHz in the E values appeared to be significant. The wild-type E value of 0.508 GHz was required to simulate the observed shoulders on the low-field resonances. As the E value was progressively reduced while keeping all of the other simulation parameters constant, the shoulders were lost, resulting in a line shape like those of the mutant.

Interaction with Substrate Analogues. The addition of azide to RcMn(II)SOD-WT led to the appearance of a sharp six-line component in the center of the spectra (between 10.17 and 10.22 T, Figure 3B). This was indicative of the formation of hexacoordinated centers with azide directly bound to the Mn(II) centers (*21*). There were also subtle changes to the other resonances that pointed to alterations in the Mn(II) zero-field interactions corresponding to the remaining pentacoordinated centers (*21*) (Figure 3C). By stark contrast, when azide was added to the Y34F mutant, there was no evidence of the formation of hexacoordinated centers (Figure 3B). However, small changes in the resonances associated with the pentacoordinated centers were observed in each spectrum (Figure 3D). This perturbation was evident from the narrowing of the low field lines of the spectrum by about 0.8 mT (Figure 3D). In the case of the wild type, the effect of azide on the spectrum of the pentacoordinated sites was even smaller (Figure 3C).

Distinct from azide, fluoride addition had a strong effect on the pentacoordinated centers of RcMn(II)SOD-WT, but it did not form any hexacoordinated centers (*21*) (Figure 3B). In the case of the mutant protein, fluoride addition produced no measurable effect on the spectrum (Figure 3B and D).

Temperature-Dependent Transition. The incubation of *E. coli* Mn(II)SOD at temperatures between 240 and 273 K prior to flash-freezing in liquid nitrogen has been shown to lead to the appearance of a six-line component in the middle of the HFEPR spectra, the magnitude of which was temperature dependent. This demonstrated that there was a temperature-dependent equilibrium between hexa and pentacoordinated centers (*40*). The same phenomenon was observed for both wild-type and mutant RcMn(II)SOD proteins (Figure 4). The intensity of the six-line component increased with decreasing incubation temperature and was completely reversible on warming. As with *E. coli* MnSOD, equilibration between the hexa and pentacoordinated forms took progressively longer periods of time with decreasing temperature, taking up to 48 h at 240 K for both the wild-type and mutant proteins. Samples used to measure the relative amounts of the two forms were incubated for 72 h to ensure that they were well equilibrated. For a given temperature, the normalized intensity of the six-line component was bigger for the RcMn(II)SOD-Y34F than for the wild-type enzyme. Each spectrum was then decomposed into two components, in the same manner as that we had previously done for the *E. coli* Mn(II)SOD (*40*). From the resulting data, the equilibrium constant, defined as the ratio of the hexacoordinated to pentacoordinated forms, at each temperature was estimated, and a van't Hoff plot was constructed (Figure 5). From this thermodynamic analysis, the enthalpy and entropy for the equilibrium were estimated. The values for RcMn(II)SOD-WT were -4.7 ± 0.5 Kcal·mol^{-1} and -21 ± 2 cal·mol^{-1}·K^{-1} for ΔH and ΔS, respectively, very close to the reported values for the same transition in EcMn(II)SOD (*21*). For RcMn-(II)SOD-Y34F, the values were -12 ± 2 Kcal·mol^{-1} and -53 ± 7 cal·mol^{-1}·K^{-1} for ΔH and ΔS, respectively. Therefore, the effect of the mutation was -7 Kcal·mol^{-1} in enthalpy and -32 cal·mol^{-1}·K^{-1} in entropy.

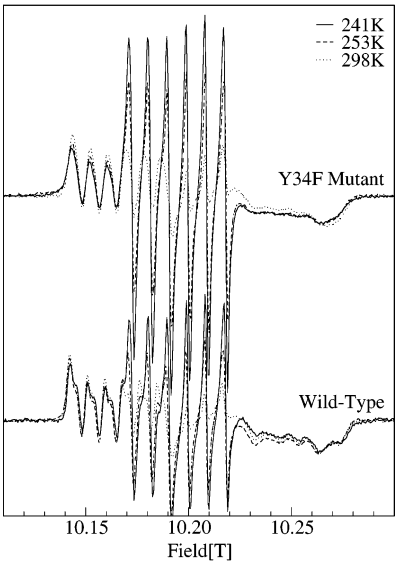

FIGURE 4: HFEPR spectra (285 GHz) of RcMn(II)SOD-WT (top) and RcMn(II)SOD-Y34F (bottom) after incubation at 241 K (—), 253 K (---), and 298 K (•••).

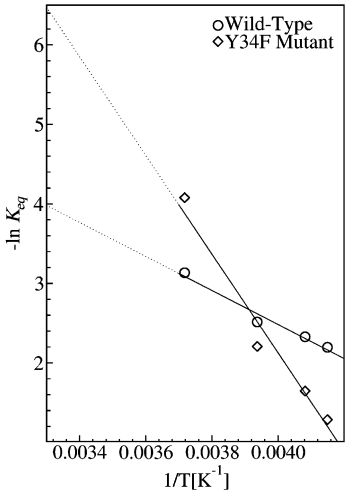

FIGURE 5: van't Hoff plot of the equilibrium constant of the five- to six-coordinated low-temperature equilibrium for the wild-type (○) and the mutant (◊) enzymes.

Electronic Absorption Properties of the Oxidized Proteins. The oxidized state of RcMnSOD-WT and RcMnSOD-Y34F were monitored with optical spectroscopy. Figure 6 shows the visible spectra of RcMnSOD-WT and RcMnSOD-Y34F. These spectra correspond to the oxidized Mn(III) centers and present the characteristic maximum around 475 nm observed previously by others for various Mn(III)SODs (*20*, *27*). In agreement with the published data for the same mutation in the *E. coli* (*20*) and human (*27*) MnSODs, the spectrum of the mutant RcMnSOD-Y34F protein was nearly identical to that of the wild-type enzyme (Figure 6). The addition of 100 mM azide induced a similar blue shift of the spectra of both wild-type and mutant proteins (Figure 6). The addition of fluoride also led to a blue shift in the spectra for both proteins, but the magnitude of the shift was much smaller than that for azide (Figure 6).

DISCUSSION

The overall purification process, electrophoretic analysis, and activity measurements suggested that RcMnSOD-Y34F folds in a correct manner and is a homodimer like the native protein (*18*). HFEPR spectroscopy also indicated that similarities in the electronic structures of native and mutant proteins extended down to the molecular level of the metal binding site. The Mn(II) zero-field interaction that dominates the HFEPR MnSOD spectra has been demonstrated to be sensitive to structural and electrostatic perturbations well beyond the primary ligand shell (*21*, *31*). Hence, the near identical HFEPR spectra of the mutant and the wild-type proteins (Figure 3A) strongly suggested that the replacement of Y34 by a phenylalanine conserved the structure and electrostatic environment of the metal site. This was entirely consistent with crystallographic studies of the same mutation in other MnSODs (*27*, *28*). However, there were also subtle differences in the HFEPR spectra induced by the mutation that were both reproducible and measurable. These differences likely arose from the modifications in the hydrogen-bonding network that normally connects Y34 to the axial solvent ligand of the metal center.

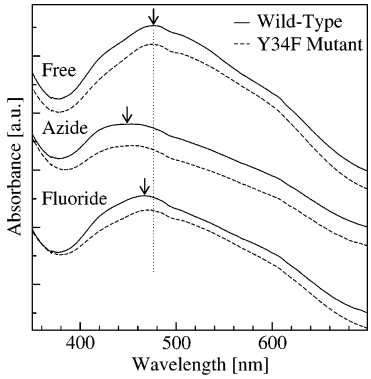

FIGURE 6: Visible absorption spectra of RcMn(II)SOD-WT (—) and RcMn(II)SOD-Y34F (---) in the absence (top, Free) or presence of 100 mM azide (middle, Azide) and 100 mM fluoride (bottom, Fluoride). The maximum for each condition is indicated by an arrow. The spectra were offset for clarity.

The fact that any changes associated with the Y34F mutation were detected at all had important consequences regarding previous studies on the pH dependence of HFEPR Mn(II)SOD spectra. It is reasonable to assume that ionization of Y34 to a negative-charge-bearing tyrosinate should have an effect at least as large as that of the Y34F mutation. However, no changes to native RcMn(II)SOD spectra were observed even above pH 11 (*21*). Hence, the present study of the Y34F mutant confirms our previous suggestion that the pK_a of Y34 in RcMn(II)SOD-WT, and by analogy in Mn(II)SODs from *P. gingivalis* and *E. coli*, must be higher than 12.

It is known that the substitution of Y34 by a phenylalanine in the human MnSOD does not modify the redox potential of this enzyme (*42*). The fact that the magnitude of the Mn(II) zero-field interaction in RcMnSOD is only slightly affected by the mutation suggests that the electronic environment of Mn(II) remains essentially unchanged and that it is unlikely that its redox potential depends on Y34. This argument is further supported by the following experimental observations. The difference in the redox potentials between the MnSOD and manganese-substituted FeSOD from *E. coli* has been measured by Vance and Miller to be more than half a volt (*43*). The magnitudes of zero-field parameters $|D|$ and E of these two proteins differ by about 100 and 500

MHz, respectively (*31*), and constitute the extremes measured thus far for Mn(II) centers in SODs. This difference is more than 10-fold larger than that between the wild-type and Y34F mutant of RcMn(II)SOD. For this reason, it is difficult to imagine that any large changes in the RcMnSOD redox potential are induced by the Y34F mutation, unless there is a large differential effect of the mutation on the reduced and oxidized states. It has already been shown that the mutation does not modify the reduction potential of the human MnSOD (*42*), and therefore, it seemed unlikely that the same mutation would do so in RcMnSOD. This meant that the lower activity of the mutant was due to some other differences.

However, the conservation of Y34 among the vast majority of FeSODs and MnSODs does appear to indicate some other important role of this residue in enzymatic activity. The Y34F mutation affected the activity of RcMnSOD more than that of any other MnSODs (*20*, *29*). The HFEPR experiments suggest that Y34 is important for anion binding to the reduced RcMnSOD enzyme. This was evident from the fact that none of the pronounced changes induced by fluoride and azide on the spectrum of the wild type were observed for the mutant protein (Figure 3B). Hence, it is likely that Y34 plays an important role in substrate binding. A conventional 9 GHz EPR spectroscopy study concluded that the same mutant of the *E. coli* MnSOD protein does bind azide and fluoride in the reduced state (*20*). However, we have demonstrated that the interpretation of 9 GHz measurements is often fraught with difficulties. For example, the addition of azide to a clean Mn(II)SOD sample containing no adventitious Mn(II) ions produced almost no changes in the 9 GHz EPR spectrum, and yet it did have a pronounced effect in the 285 GHz HFEPR spectra (see Supporting Information in ref *21*). Similarly, in contrast to HFEPR, it is difficult to discriminate non-protein-bound Mn(II) ions from those of the protein metal site in the hexacoordinated state by 9 GHz EPR spectroscopy (see Supporting Information in ref *21*). These divergent views from the EPR data of the role of Y34 are all the more striking because HFEPR shows that the wild-type *E. coli* and *R. capsulatus* Mn(II)-SOD proteins bind azide and fluoride in a similar manner and to a similar extent, which suggests that the geometry and energetics of anion binding in the two proteins must be similar. Whether the role of Y34 in small anion binding is an intrinsic property of Mn(II)SODs or specific to the *R. capsulatus* protein will need to be studied further.

In contrast to the pronounced effect that the Y34F mutation had on anion binding to the reduced form of RcMnSOD, the optical spectra of the oxidized states of the wild-type and mutant proteins showed no difference (Figure 6). This result was consistent with previous reports that have shown that the oxidized MnSODs from *E. coli* and humans harboring the same mutation (*20*, *27*) do interact with azide and fluoride in a manner similar to that of the wild type.

One explanation for the different anion binding properties of the oxidized and reduced forms may be that in the reduced state the electrostatic forces are more balanced, and Y34 functions to facilitate the transport of anions into the active site, whereas in the oxidized state, there is an inherent greater electrostatic driving force for anion−metal interaction because of the higher formal charge on the Mn(III). In the oxidized enzyme, Y34 may play the opposite role in the reduced form and help the transport of anions out of the active site. This idea is supported by the observed increase in the K_d for azide in Mn(III)SOD Y34F mutants (*19*, *20*, *22*, *29*) for which an increase in the ratio of the hexacoordinated to pentacoordinated forms has also been observed (*20*). In this electrostatic transport model, the removal of the tyrosine forces the equilibrium to disfavor anion−metal interaction in the reduced state, whereas in the oxidized state, the equilibrium is displaced in the opposite direction.

This electrostatic model for the role of Y34 is entirely consistent with our previous observations on anion binding and temperature-dependent coordination that suggest an equilibrium between two mutually exclusive binding sites (*21*, *40*). In a thermodynamic sense, this equilibrium does not imply a continuous movement of the anion through an electrostatic gradient but three different states for the protein−anion interaction (Figure 1). The first state is one that is equivalent to the protein resting state in which the active site is pentacoordinated and unperturbed by the presence of the anion in the bulk solvent (bulk solvent, Figure 1). An intermediate state is one in which an azide or fluoride, or another molecule, is in the superoxide access channel (distal site, Figure 1) and exerts a weak electrostatic influence on the Mn(II) electronic structure. This state is manifested in the 0.15 T-wide HFEPR spectrum of the five-coordinated Mn(II)SOD by changes of a few milliteslas in the widths and positions of the resonances (*21*). Analysis of such changes in the *E. coli* MnSOD spectra based on a simple electrostatic model of the Mn(II) zero-field interaction predicted that the distal site was about 5 Å from the Mn(II) ion (*21*). For RcMn(II)SOD-WT, anions at the distal state exerted a weaker perturbation than that measured for the *E. coli* protein, suggesting that the site was further away or oriented differently with respect to the Mn(II) binding site (*21*). (It is important to note that electrostatic interactions are dipolar and that the effects of distance and angular orientation cannot be distinguished.) Although spectroscopic perturbation due to the distal site was weak, its influence was clearly manifested in the titration experiments in which complete direct anion binding could not be achieved. Azide did have a small perturbative effect on Mn(II) on zero-field in Y34F mutant, whereas the fluoride had none (Figure 3D). This suggested that Y34 may not be the only residue that defines the distal site and that others are involved.

Finally, the third state is the one in which the extra ligand is within bonding distance of the Mn(II) ion (proximal site, Figure 1). We have argued that in this proximal state, azide can directly coordinate the metal center as a sixth ligand, whereas the fluoride anion is too small to both hydrogen-bond Y34 and ligate the metal ion but is very close to the metal (*21*). The Mn(II) HFEPR spectra of the anions occupying the proximal site were distinct from that of the wild-type native protein (*21*) (Figure 3B). Therefore, the lack of any effect in the Y34F mutant made it clear that neither azide nor fluoride occupied the proximal state, at least not to any detectable levels (Figure 3B).

The same model used for azide and fluoride binding can be use to rationalize the observed low-temperature pentacoordinated-to-hexacoordinated transition (*40*). Because this transition occurred in absence of any exogenous ligand, we attributed this to the movement of a water molecule into the proximal state (*40*). In the resting state of the protein at room

temperature, a water molecule lies in the distal state, as is seen in crystal structures of native MnSODs (*44*, *45*) and also the Y34F mutants (*27*, *28*). If our assignment is correct, this water molecule in fact exists in an equilibrium defined by the distal and proximal states. The thermodynamic analysis indicated that for the wild-type protein ΔH and ΔS were very close to the values previously determined for the *E. coli* Mn(II)SOD (-5 ± 1 kcal/mol and -24 ± 5 cal/mol·K) (*40*), but for the mutant, RcMn(II)SOD-Y34F, both values were significantly lower. This difference in free energy between the wild type and mutant implies that Y34 partially controls the low-temperature equilibrium. Moreover, the difference in enthalpy is very close to that expected for a hydrogen bond between a water molecule and a tyrosine residue (*21*, *46*, *47*). Thus, the shift in enthalpy in the mutant further supports our suggestion that the sixth ligand at low temperatures is in fact the proposed water molecule that is seen in the crystallographic structures that hydrogen bonds Y34 (*44*, *45*).

An extrapolation of the van't Hoff plot (Figure 5) shows that at room temperature the equilibrium constant (K_{eq}, Figure 1) between the water-bound distal and proximal states would be 10-fold lower in the RcMn(II)SOD-Y34F than in RcMn-(II)SOD-WT. This 10-fold decrease in K_{eq} could partially explain the highly attenuated effect of fluoride and azide on the mutant HFEPR spectra. If a similar 10-fold reduction is assumed for these anions, the K_{eq} between the distal and proximal states would be 0.03 M^{-1} for azide and 0.1 M^{-1} for fluoride, according to our previous results (*21*). Such a low K_{eq} would put the proximal state for both anions at the limits of detection, and just an additional small reduction in the binding constant (K_d, Figure 1) could easily explain why azide and fluoride appear to not interact with RcMn(II)SOD-Y34F. This difference in K_d is not valid for the water molecule because it is a ubiquitous neutral molecule and is already present in the access channel. However, azide and fluoride are negatively charged and their concentrations in the solution are much lower. Hence, the interaction with Y34 is likely to be required in the first place as a driving force to pull these analogues from the bulk solvent to the substrate access channel. There are two obvious questions: (1) What happens with superoxide, which is also negatively charged? (2) Why is the mutant protein still active? Our electrostatic model presumably applies to all anions that are sufficiently small to enter the access channel and migrate between the distal and proximal positions. However, we cannot rigorously exclude the possibility that superoxide does not experience additional interactions. Given our knowledge of the structure of MnSOD, it is difficult to imagine what such interactions may be, especially because the Y34F mutation inhibits the binding of a linear anion that is larger than superoxide and also an anion that is smaller. If one assumes that there are no such additional specific interactions and that the superoxide anion must be in the proximal position in order to be reduced to peroxide, then a decrease in K_{eq} for superoxide by a factor of 10 would lead to a slower but still active enzyme. This is consistent with Greenleaf and co-workers (*48*) who have observed that the reduction of superoxide to peroxide is the most affected step in the catalytic cycle of the human Y34F MnSOD mutant. It should also be noted that our model is based on thermodynamic equilibria and says nothing about the kinetics of the processes. Hence, even if the equilibrium were completely displaced toward the distal state but the kinetics between both states were sufficiently fast, the protein would still be capable of performing catalysis. The replacement of Y34 may not eliminate all of the electrostatic forces that would drive anions, including superoxide, toward the active site. Hence, even if the mutant protein has less control over superoxide traffic, it would be possible for the enzyme to still cause disproportionate levels of superoxide just by passive diffusion.

R. capsulatus SOD has been formally classified as a cambialistic-SOD (*18*). However, it shows much higher activity with Mn than Fe and its reduced Mn form behaves in the same fashion as the pure Mn-type SOD from *E. coli* with respect to azide and fluoride interactions and low-temperature incubation (*21*, *40*). Hence, it is likely that the results presented here also apply to MnSODs in general. To the best of our knowledge, this is the first detailed study of the reduced state of this mutation in a MnSOD. We propose that Y34 is essential for translocating the superoxide anion from the distal site, that is solvent exposed, to the proximal, catalytic, position.

ACKNOWLEDGMENT

We are grateful to Diana Kiriovsky, Adjele Wilson, and Thanh-Lan Lai for technical assistance.

REFERENCES

1. Fridovich, I. (1995) Superoxide radical and superoxide dismutases, *Annu. Rev. Biochem. 64*, 97−112.
2. Touati, D. (1997) Superoxide Dismutases in Bacteria and Pathogen Protists, in *Oxidative Stress and the Molecular Biology of Antioxidant Defenses* (Scandalios, J. G., Ed.) pp 447−493, Cold Spring Harbor Laboratory Press, NY.
3. Bull, C., and Fee, J. A. (1985) Steady-state kinetic studies of superoxide dismutases: properties of the iron containing protein from *Escherichia coli*, *J. Am. Chem. Soc. 107*, 3295−3304.
4. Lavelle, F., McAdam, M. E., Fielden, E. M., and Roberts, P. B. (1977) A pulse-radiolysis study of the catalytic mechanism of the iron-containing superoxide dismutase from *Photobacterium leiognathi*, *Biochem. J. 161*, 3−11.
5. Klug-Roth, D., Fridovich, I., and Rabani, J. (1973) Pulse radiolytic investigations of superoxide catalyzed disproportionation. Mechanism for bovine superoxide dismutase, *J. Am. Chem. Soc. 95*, 2786−2790.
6. Kim, E. J., Chung, H. J., Suh, B., Hah, Y. C., and Roe, J. H. (1998) Transcriptional and post-transcriptional regulation by nickel of sodN gene encoding nickel-containing superoxide dismutase from *Streptomyces coelicolor* Muller, *Mol. Microbiol. 27*, 187−195.
7. Kim, F. J., Kim, H. P., Hah, Y. C., and Roe, J. H. (1996) Differential expression of superoxide dismutases containing Ni and Fe/Zn in *Streptomyces coelicolor*, *Eur. J. Biochem. 241*, 178−185.
8. Stroupe, M. E., DiDonato, M., and Tainer, J. A. (2001) In *Handbook of Metalloproteins* (Messerschmidt, A., Huber, R., Wieghardt, K., and Paulos, T., Eds.) pp 941−951, Wiley and Sons, Chicester, U.K.
9. Miller, A.-F. (2001) In *Handbook of Metalloproteins* (Messerschmidt, A., Huber, R., Wieghardt, K., and Paulos, T., Eds.) pp 668−682, Wiley and Sons, Chicester, U.K.
10. Sugio, S., Hiraoka, B. Y., and Yamakura, F. (2000) Crystal structure of cambialistic superoxide dismutase from *Porphyromonas gingivalis*, *Eur. J. Biochem. 267*, 3487−3495.
11. Schmidt, B., Meier, B., and Parak, F. (1996) X-ray structure of the cambialistic superoxide dismutase from *Propionibacterium shermanii* active with Fe or Mn, *J. Biol. Inorg. Chem. 1*, 532−541.
12. Ose, D. E., and Fridovich, I. (1976) Superoxide dismutase. Reversible removal of manganese and its substitution by cobalt, nickel or zinc, *J. Biol. Chem. 251*, 1217−1218.

13. Yamakura, F. (1980) Cadmium, chromium, and manganese replacement for iron in iron-superoxide dismutase from *Pseudomonas ovalis*, *J. Biochem. (Tokyo) 88*, 191−196.
14. Meier, B., Barra, D., Bossa, F., Calabrese, L., and Rotilio, G. (1982) Synthesis of either Fe- or Mn-superoxide dismutase with an apparently identical protein moiety by an anaerobic bacterium dependent on the metal supplied, *J. Biol. Chem. 257*, 13977−13980.
15. Amano, A., Shizukuishi, S., Tamagawa, H., Iwakura, K., Tsunasawa, S., and Tsunemitsu, A. (1990) Characterization of superoxide dismutase purified from either anaerobically maintained or aerated *Bacteroides gingivalis*, *J. Bacteriol. 172*, 1457−1463.
16. Martin, M. E., Byers, E. B. R., Olson, M. O. J., Salin, M. L., Arceneaux, J. E. L., and Tolbert, C. (1986) A *Streptococcus mutans* superoxide dismutase that is active with either manganese or iron as a cofactor, *J. Biol. Chem. 261*, 9361−9367.
17. Gregory, E. M. (1985) Characterization of the O_2-induced manganese-containing superoxide dismutase from *Bacteroides fragilis*, *Arch. Biochem. Biophys. 238*, 83−89.
18. Tabares, L. C., Bittel, C., Carrillo, N., Bortolotti, A., and Cortez, N. (2003) The single superoxide dismutase of *Rhodobacter capsulatus* is a cambialistic, manganese-containing enzyme, *J. Bacteriol. 185*, 3223−3227.
19. Miller, A. F., Sorkin, D. L., and Padmakumar, K. (2005) Anion binding properties of reduced and oxidized iron-containing superoxide dismutase reveal no requirement for tyrosine 34, *Biochemistry 44*, 5969−5981.
20. Whittaker, M. M., and Whittaker, J. W. (1997) Mutagenesis of a proton linkage pathway in *Escherichia coli* manganese superoxide dismutase, *Biochemistry 36*, 8923−8931.
21. Tabares, L. C., Cortez, N., Hiraoka, B. Y., Yamakura, F., and Un, S. (2006) Effects of substrate analogues and pH on manganese superoxide dismutases, *Biochemistry 45*, 1919−1929.
22. Lah, M. S., Dixon, M. M., Pattridge, K. A., Stallings, W. C., Fee, J. A., and Ludwig, M. L. (1995) Structure-function in *Escherichia coli* iron superoxide dismutase: comparisons with the manganese enzyme from *Thermus thermophilus*, *Biochemistry 34*, 1646−1660.
23. Schmidt, M. (1999) Manipulating the coordination number of the ferric iron within the cambialistic superoxide dismutase of *Propionibacterium shermanii* by changing the pH-value. A crystallographic analysis, *Eur. J. Biochem. 262*, 117−127.
24. Whittaker, J. W., and I., S. E. (1988) Spectroscopic studies on ferrous non-heme iron active sites: magnetic circular dichroism of mononuclear Fe sites in superoxide dismutase and lipoxygenase, *J. Am. Chem. Soc. 110*, 5329−5339.
25. Whittaker, M. M., and Whittaker, J. W. (1996) Low-temperature thermochromism marks a change in coordination for the metal ion in manganese superoxide dismutase, *Biochemistry 35*, 6762−6770.
26. Jackson, T. A., Karapetan, A., Miller, A.-F., and Brunold, T. C. (2004) Spectroscopic and computational studies of the azide-adduct of manganese superoxide dismutase: definitive assignment of the ligand responsible for the low-temperature thermochroism, *J. Am. Chem. Soc. 126*, 12477−12491.
27. Guan, Y., Hickey, M. J., Borgstahl, G. E. O., Hallewell, R. A., Lepock, J. R., O'Conner, D., Hsieh, Y., Nick, H. S., Silvermann, D. N., and Tainer, J. A. (1998) Crystal structure of Y34F mutant human mitochondrial manganese superoxide dismutase and the functional role of tyrosine 34, *Biochemistry 37*, 4722−4730.
28. Edwards, R. A., Whittaker, M. M., Whittaker, J. W., Baker, E. N., and Jameson, G. B. (2001) Removing a hydrogen bond in the dimer interface of *Escherichia coli* manganese superoxide dismutase alters structure and reactivity, *Biochemistry 40*, 4622−4632.
29. Hunter, T., Ikebukuro, K., Bannister, W. H., Bannister, J. V., and Hunter, G. J. (1997) The conserved residue tyrosine 34 is essential for maximal activity of iron-superoxide dismutase from *Escherichia coli*, *Biochemistry 36*, 4925−4933.
30. Un, S., Dorlet, P., Voyard, G., Tabares, L. C., and Cortez, N. (2001) High-field EPR characterization of manganese reconstituted superoxide dismutase from *Rhodobacter capsulatus*, *J. Am. Chem. Soc. 123*, 10123−10124.
31. Un, S., Tabares, L. C., Cortez, N., Hiraoka, B. Y., and Yamakura, F. (2004) Manganese(II) zero-field interaction in cambialistic and manganese superoxide dismutases and its relationship to the structure of the metal binding site, *J. Am. Chem. Soc. 126*, 2720−2726.
32. Whittaker, M. M., and Whittaker, J. W. (1991) Active site spectral studies on manganese superoxide dismutase, *J. Am. Chem. Soc. 113*, 5528−5540.
33. Gasteiger, E., Hoogland, C., Gattiker, A., Duvaud, S., Wilkins, M. R., Appel, R. D., and Bairoch, A. (2005) Protein Identification and Analysis Tools on the ExPASy Server, in *The Proteomics Protocols Handbook* (Walker, J. M., Ed.) pp 571−607, Humana Press, Totowa, NJ.
34. Goldring, J. P. D., and Ravaioli, L. (1996) Solubilizarion of protein-dye complexes on nitrocellulose to quantify proteins spectrophotometrically, *Anal. Biochem. 242*, 197−201.
35. Bradford, M. M. (1976) A rapid and sensitive method for the quantitation of microgram quantities of protein utilizing the principle of protein-dye binding, *Anal. Biochem. 72*, 248−254.
36. McCord, J. M., and Fridovich, I. (1969) Superoxide dismutase. An enzymic function for erythrocuprein (hemocuprein), *J. Biol. Chem. 244*, 6049−6055.
37. Beauchamp, C., and Fridovich, I. (1971) Superoxide dismutase: improved assays and an assay applicable to acrylamide gels, *Anal. Biochem. 44*, 276−287.
38. Un, S., Dorlet, P., and Rutherford, A. W. (2001) A high-field tour of radicals in photosystems I and II, *Appl. Magn. Reson. 21*, 341−361.
39. Burghaus, O., Plato, M., Rohrer, M., Moebius, K., MacMillan, F., and Lubitz, W. (1993) 3-mm High-field EPR on semiquinone radical anions Q($*^-$) related to photosynthesis and on the primary donor P($*^+$) and acceptor QA($*^-$) in reaction centers of *Rhodobacter sphaeroides* R-26, *J. Phys. Chem. 97*, 7639−7647.
40. Tabares, L. C., Cortez, N., Agalidis, I., and Un, S. (2005) Temperature-dependent coordination in *E. coli* manganese superoxide, *J. Am. Chem. Soc. 127*, 6039−6047.
41. Donahue, J. L., Okpodu, C. M., Cramer, C. L., Grabau, E. A., and Alscher, R. G. (1997) Responses of antioxidants to paraquat in pea leaves (relationships to resistance), *Plant Physiol. 113*, 249−257.
42. Leveque, V., J.-P., Vance, C. K., Nick, H. S., and Silverman, D. N. (2001) Redox properties of human manganese superoxide dismutase and active-site mutants, *Biochemistry 40*, 10586−10591.
43. Vance, C. K., and Miller, A. F. (2001) Novel insights into the basis for *Escherichia coli* superoxide dismutase's metal ion specificity from Mn-substituted FeSOD and its very high E(m), *Biochemistry 40*, 13079−13087.
44. Borgstahl, G. E., Parge, H. E., Hickey, M. J., Beyer, W. F. J., Hallewell, R. A., and Tainer, J. A. (1992) The structure of human mitochondrial manganese superoxide dismutase reveals a novel tetrameric interface of two 4-helix bundles, *Cell 71*, 107−118.
45. Edwards, R. A., Baker, H. M., Whittaker, M. M., Whittaker, J. W., Jameson, G. B., and Baker, E. N. (1998) Crystal structure of *Escherichia coli* manganese superoxide dismutase at 2.1 Å resolution, *J. Biol. Inorg. Chem. 3*, 161−171.
46. Schütz, M., Bürgi, T., Leutwyler, S., and Fischer, T. (1993) Intermolecular bonding and vibrations of phenol H_2O (D_2O), *J. Chem. Phys. 98*, 3763−3776.
47. Cleland, W. W., Frey, P. A., and Gerlt, J. A. (1998) The low barrier hydrogen bond in enzymatic catalysis, *J. Biol. Chem. 273*, 25529−25532.
48. Greenleaf, W. B., Perry, J. J., Hearn, A. S., Cabelli, D. E., Lepock, J. R., Stroupe, M. E., Tainer, J. A., Nick, H. S., and Silverman, D. N. (2004) Role of hydrogen bonding in the active site of human manganese superoxide dismutase, *Biochemistry 43*, 7038−7045.

BI700438J